EurJIC
European Journal of Inorganic Chemistry

Full Paper
doi.org/10.1002/ejic.201901304

Chemistry Europe
European Chemical Societies Publishing

Nitrogen Photoactivation

SPECIAL ISSUE

Multi-Tier Electronic Structure Analysis of Sita's Mo and W Complexes Capable of Thermal or Photochemical N_2 Splitting

Severine Rupp,[a] Felix Plasser,*[b] and Vera Krewald*[a]

Abstract: An emerging approach for the activation of the nitrogen molecule is the light-driven splitting of the N–N bond. Less than ten examples for complexes capable of N_2 photoactivation are currently known, and the underlying photophysical and photochemical processes after light absorption are largely unresolved. All complexes have a central [M(μ-η^1:η^1-N_2)M] unit with equivalent ligand spheres around each metal. For several of these complexes, small modifications of the ligand sphere result in thermal rather than photochemical activity. Herein, we analyse the electronic structures and computed UV/Vis spectra of four complexes: two thermally and two photochemically active complexes, each either involving molybdenum or tungsten. The analysis of electronic structures and spectra is based on the molecular orbitals, difference densities and the charge-transfer numbers provided by TheoDORE. We find that the spectra of the photochemically active complexes contain excitations with more ligand-to-metal charge-transfer character and higher intensity, providing a plausible explanation for light-induced nitrogen splitting.

Introduction

Computational chemists are often tasked with the analysis of electronic transitions in UV/Vis spectra computed with time-dependent density functional theory (TD-DFT) or other quantum chemistry methods. Such analyses are aimed at revealing structure–property relationships intended to complement experiment. Conventionally, the analysis of TD-DFT-derived spectra would be based on the contributions of individual one-electron transitions to each excited state. While in simple cases, analyses based on individual molecular orbital (MO) contributions will be sufficient, in transition metal complexes the situation is oftentimes more complicated. In particular for multinuclear complexes with covalent bonding situations, the unequivocal assignment of transitions is hindered by the inherently strong mixing of metal and ligand orbitals. As a complementary resource, transition densities and difference densities can be computed and analyzed for each state. Similar to the MOs, the transition and difference densities can appear as convoluted surfaces and their interpretation may be – at least to some extent – subject to the biases and views of the researchers. For a more objective interpretation of transitions, the TheoDORE program makes use of the one-electron transition density matrix.[1] The user chooses a fragmentation pattern for the molecule, e.g. based on functional groups or ligands, and the character of the excitations is interpreted in terms of Frenkel excitonic states or charge separated states, both of which can be localized or delocalized with respect to the chosen fragments. In this contribution, we use these three tiers of electronic structure analysis, i.e. MO analysis, difference density analysis, and TheoDORE analysis, to obtain a better understanding of molybdenum and tungsten complexes with linear [M(μ-η^1:η^1-N_2)M] cores. Based on these analyses, we identify electronic structure characteristics associated with either photochemical or thermochemical reactivity of these complexes.

The analysis of computed UV/Vis spectra is of particular importance for photochemically active transition metal complexes. An emerging approach in nitrogen activation chemistry is the use of light to cleave the strong N–N bond.[2] Nitrogen fixation is of course a very active and topical field of research:[3] a better understanding of nitrogen fixation in nature is sought,[4] synthetic approaches to nitrogen activation or splitting are devised,[5] heterogeneous and homogeneous catalysts are studied,[6] and computational studies help to obtain more detailed mechanistic insights.[7] When discussing the overall goal of nitrogen fixation chemistry using molecular approaches, two targets can be distinguished: (i) activation and sequential protonation of N_2, usually bound in metal complexes as an end-on or bridging species, leading to NH_3,[6a,8] and (ii) complete splitting of N_2, so far only known for homometallic, symmetric transition metal dimers, leading to metal nitrido[9] intermedi-

[a] *Fachbereich Chemie, Theoretische Chemie, Technische Universität Darmstadt,*
Alarich-Weiss-Str. 4, 64287 Darmstadt, Germany
E-mail: krewald@chemie.tu-darmstadt.de
https://www.chemie.tu-darmstadt.de
[b] *Department of Chemistry, Loughborough University,*
Loughborough, LE11 3TU, United Kingdom
E-mail: f.plasser@lboro.ac.uk
https://fplasser.sci-public.lboro.ac.uk
Supporting information and ORCID(s) from the author(s) for this article are available on the WWW under https://doi.org/10.1002/ejic.201901304.

Full Paper
doi.org/10.1002/ejic.201901304

ates that can be protonated to form NH_3[10] or reacted with more complex reagents to incorporate the N-atom into higher-value molecules.[6a,11]

For the approach of splitting the N_2 molecule with light, only a small number of molecular complexes are currently known (see Figure 1a)[12] alongside several heterogeneous systems.[13] Structurally and in terms of their properties, the molecular complexes are remarkably similar to thermochemically and electrochemically active ones.[6e,14] In some cases, the same complex[12b,15] or complexes with relatively small modifications of the ligand sphere[12f,14e,16] may be capable of thermal *and* photochemical activation. Presently, however, a detailed understanding of their photophysics and photochemistry is lacking: a study of the processes after excitation with light is only available for the thermally and photochemically active Cummins complex.[12b,15] Two other studies on the photophysics of a different molybdenum dimer that does not cleave the N–N bond upon irradiation are available.[4c,17] Computational chemistry is contributing towards elucidating the electronic structures and a more complete understanding of the photochemical processes.[2,12f,16b,18] At this point, however, a general route towards complexes capable of N_2 photosplitting is not known, nor is it possible to predict from a structure or ground state electronic configuration whether a complex will be photoactive towards nitrogen cleavage. With so few examples available and given the dearth of time-resolved spectroscopic data, any attempt to generalize the findings will most probably be incomplete. It appears likely that several different routes can lead to light-induced dinitrogen bond splitting. Paralleling the two targets of nitrogen fixation chemistry, i.e. production of ammonia vs. generation of metal nitrido complexes, two different photoactivation paths can be envisaged (Figure 1b):[2] (i) excitation into N–N π^* orbitals, leading to a weakened π-bond and hence a geometrically more flexible μ-N_2 bridge coupled to the onset of lone pair formation, and (ii) excitation into a N–N σ^* orbital, which may lead to a complete splitting of the μ-N_2 bridge.

We emphasize that such a simplified molecular orbital picture does not do justice to the complexity of transition metal photochemistry and the multireference character the involved electronically excited states will likely have. However, it may provide some guidance for identifying potentially photoactive excitations in the UV/Vis spectra of dinitrogen-bridged complexes. For a complete understanding of the photochemistry, the post-excitation dynamics must be studied computationally and experimentally, e.g. with wavepacket or *ab initio* excited state dynamics in combination with time-resolved UV/Vis spectroscopy.[19] Nonetheless, a detailed analysis of the wavefunctions at the ground state geometry may provide at least a rough guidance in terms of the possible photochemical pathways at a significantly lower computational cost, e.g. by objectively identifying excited states with strong contributions on the nitrogen bridge or relevant types of charge transfer character.

When aiming to understand the differences between photochemically and thermally active N_2-splitting complexes, a series of transition metal dimers with a central [M(μ-N_2)M] motif by Sita is of particular note. The entire series encompasses the metals Ti,[14b] Zr,[20] Hf,[20] V,[21] Nb,[21] Ta,[22] Mo,[12e,14b,16a,23] and

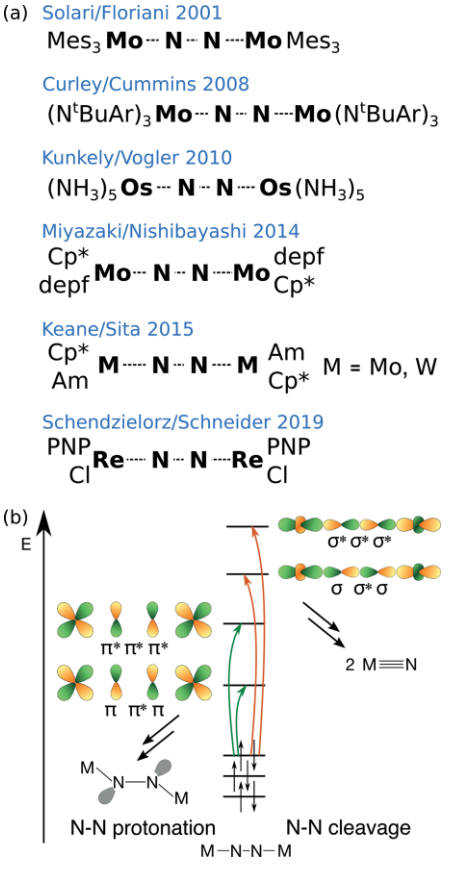

Figure 1. (a) Sketches of currently known dinitrogen photoactivation complexes,[12a–12f] see also Ref.[12g]. The ligand abbreviations stand for Mes: 1,3,5-trimethylbenzene, N^{t}BuAr: anilide ligand where Ar: 3,5-$C_6H_3Me_2$, depf: 1,1′-bis(diethylphosphino)ferrocene, Cp*: pentamethylcyclopentadiene, Am: amidinate with the formula N(^{i}Pr)C(Me)N(^{i}Pr), PNP: pincer with the formula HN($CH_2CH_2P^iPr_2$)$_2$. (b) Simplified molecular orbital picture of excitations that may lead to nitrogen protonation or splitting of the μ-N_2 bridge.

W,[12e,14b,16a,23a,23b] where each metal is bound to one amidinate (Am) ligand and one pentamethylcyclopentadienyl (Cp*) ligand. For the Mo and W complexes, the substituents of the Am ligand control whether the complex is photochemically or thermally active. Succinctly expressed by Sita as "Steric Switching", the bulkier complexes with (N(*i*Pr)C(Me)N(*i*Pr))$^-$ ligands are photoactive, the less bulky complexes with (N(Et)C(Ph)N(Et))$^-$ ligands react thermally.[16]

The Sita series thus allows an investigation of electronic structures and identification of any inherent differences that control the mode of activation as well as the thermodynamics and kinetics. In previous work we found that the thermodynamics of the isomerization path from the linear [M(μ-η^1:η^1-N_2)M] core to the diamond-shaped [M(μ-N)$_2$M] core is indeed less favorable for the bulkier system.[16b] At the same time, dispersion interactions were found to stabilize the bis-μ-N molybdenum dimer product of the thermal path to such an extent that without them the reaction would be endergonic.[16b] It is worth noting that for the product of the photochemical path it was not even possible to find a stable structure when dispersion corrections were not included. With regards to energy and nature of the photochemically active states, a cluster of low-intensity

Full Paper
doi.org/10.1002/ejic.201901304

transitions was identified in the photochemically active species that had no equivalent in the thermally active compound.[16b]

In order to better understand whether the observed difference in reactivity is dominated by electronic or steric effects, the electronic structures of two thermally and two photochemically active complexes, each either involving Mo or W, are analyzed here (see Figure 2). While in open-shell complexes, a first impression of the electronic structure can be gleaned from a spin population analysis, a computational investigation of the Sita complexes with closed-shell singlet ground states is less straightforward. Besides a comparison of the molecular orbital schemes we use an analysis and interpretation of computed UV/Vis spectra to obtain insights into electronic structure differences that are otherwise difficult to evaluate.

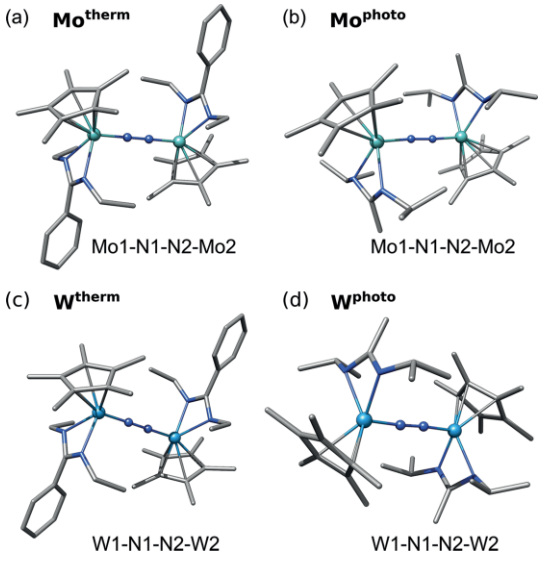

Figure 2. Geometry-optimized structures of the four complexes studied, (a) **Mo^{therm}**, (b) **Mo^{photo}**, (c) **W^{therm}** and (d) **W^{photo}**. The atomic labels for the central M-N-N-M core are shown below each complex. The Mo atoms are colored light turquoise, the W atoms light blue, the N atoms dark blue and the C atoms grey; hydrogen atoms are omitted for clarity.

Results

Structures

The complexes of interest are two thermally active complexes, $\{(\eta^5\text{-}C_5Me_5)[N(Et)C(Ph)N(Et)]M\}_2(\mu\text{-}N_2)$, further referred to as **Mo^{therm}** and **W^{therm}**, and two photochemically active complexes **Mo^{photo}** and **W^{photo}** with a less bulky amidinate ligand, $\{(\eta^5\text{-}C_5Me_5)[N(i\text{Pr})C(Me)N(i\text{Pr})]M\}_2(\mu\text{-}N_2)$, see Figure 2. Starting from the crystal structures where available, the geometries were optimized with the BP86 density functional including dispersion corrections and solvation effects for benzene, see Computational Details. Key structural parameters of the central linear $M_2(\mu\text{-}\eta^1\text{:}\eta^1\text{-}N_2)$ units are shown in Table 1. Previous work showed that the structures of the two molybdenum complexes that are capable of thermal and photochemical N_2 splitting, **Mo^{therm}** and **Mo^{photo}**, are nearly identical.[16b] Overall, the tungsten complexes have similar structural characteristics. The N–N distances are slightly longer (ca. 0.01 Å) and the M-M separation is similarly elongated, however these differences are very subtle and should not be overinterpreted.

Table 1. Key structural parameters and computed Mayer bond orders of the four complexes **Mo^{therm}**, **Mo^{photo}**, **W^{therm}** and **W^{photo}**. Interatomic distances d and average distances between metal and directly bound ligand atoms d_{av} are given in Å, angles α and dihedral angles θ are given in degrees. Bond orders are taken from LC-BLYP/def2-TZVP calculations, see Supporting Information (Table S1) for data from other functionals.

Structural Parameter	Mo^{therm}	Mo^{photo}	W^{therm}	W^{photo}
d(M1, M2)	4.863	4.855	4.879	4.875
d(N1, N2)	1.247	1.246	1.259	1.260
d(M1, N1)	1.808	1.805	1.810	1.808
d(M2, N2)	1.808	1.805	1.810	1.808
d_{av}(M1, N_{Am})	2.134	2.141	2.142	2.149
d_{av}(M2, N_{Am})	2.134	2.140	2.142	2.149
d_{av}(M1, C_{Cp^*})	2.311	2.330	2.318	2.341
d_{av}(M2, C_{Cp^*})	2.311	2.331	2.318	2.341
α(M1, N1, N2)	179.1	176.3	179.0	176.5
α(M2, N2, N1)	179.1	176.7	179.1	176.5
θ(M1, N1, N2, M2)	178.2	–152.6	179.3	179.9
B.O.(N1, N2)	1.40	1.36	0.67	0.67
B.O.(M1, N1)	1.56	1.56	2.00	2.00
B.O.(M2, N2)	1.56	1.56	2.00	2.00

A more striking difference is seen in the computed Mayer bond orders, see Table 1. In the molybdenum complexes, the bond order of the nitrogen bridge is significantly higher than in the tungsten complexes (1.4 vs. 0.7). Accordingly, the Mo–N bonds are weaker (bond order of ca. 1.6) than the W–N bonds (bond order of ca. 2.0). This observation holds across a variety of density functionals, see Table S1.

Generalized MO Scheme

Based on linear combinations of the five metal d-orbitals and three nitrogen p-orbitals of the valence region, four orbitals of σ-character (σ-σ-σ, σ-σ*-σ, σ*-σ-σ*, σ*-σ*-σ*, where each symbol characterizes the sequence of M-N, N-N and N-M interactions with the asterisk indicating antibonding character), eight orbitals of π-character (degenerate sets of π–π–π, π–π*–π, π*–π–π*, π*–π*–π*), and four orbitals of δ-character ($\delta_{xy}/\delta_{xy}^*$; $\delta_{x2-y2}/\delta_{x2-y2}^*$) can be constructed, see Figure 3a.[18b,24] The DFT calculations provide insights into the differences between the molecular orbital scheme of the four complexes, see Figure 3b. A comparison of the idealized scheme that completely neglects the surrounding ligand sphere with the orbitals obtained from DFT shows that the mixing with orbitals from the surrounding ligand sphere can be significant.

Generally, orbitals of the same character are found at similar energies across all complexes. In all cases, the σ-σ-σ, π–π–π, π–π*–π and the lower set of δ/δ*-orbitals are doubly occupied. The highest occupied molecular orbital (HOMO) and HOMO–1 are the δ/δ*-orbitals, and the lowest unoccupied molecular orbital (LUMO) and LUMO+1 are of π*–π–π* character. From Figure 3b, it is readily seen that the HOMO-LUMO gap is larger in the tungsten complexes than in the molybdenum complexes. We note that the assigned character of the unoccupied orbitals should be treated with some caution, not only due to the inherent limitations of DFT but also because in the calculations the

Full Paper
doi.org/10.1002/ejic.201901304

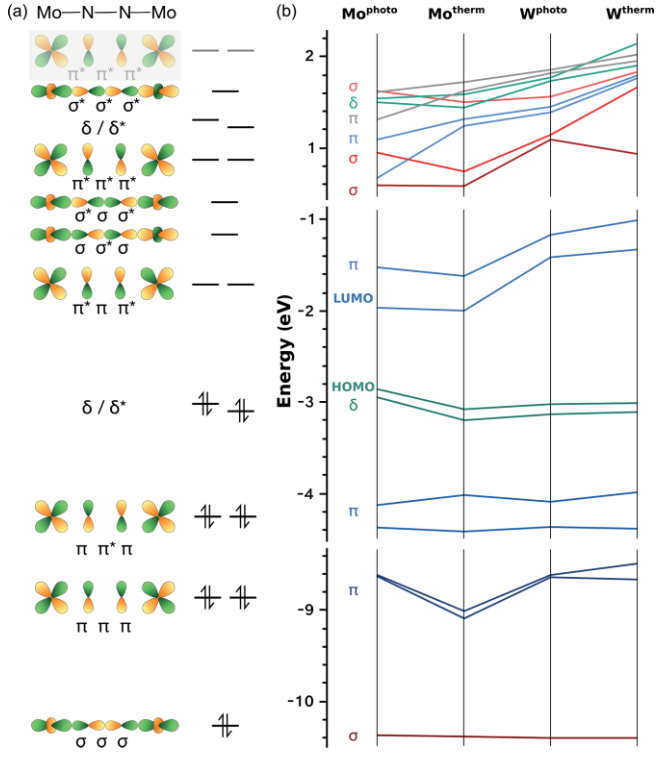

Figure 3. (a) Generalized molecular orbital scheme for the Sita complexes with linear M-N-N-M cores; the greyed-out π*–π*–π*-orbitals arise from admixture of ligand orbital character. (b) MO energy diagrams for all four complexes; the type of orbital is designated with σ/π/δ-labels and the character corresponds approximately to the MO sketched in (a) at the same height. The contour plots of the MOs for all four complexes are shown in the Supporting Information, Figures S1–S4, together with their energies. Note that we do not show any energy levels of predominantly ligand-based orbitals here.

nitrogen s- and p-orbitals on the bridge mix, leading to several possible linear combinations. The relevant orbitals are show in the Supporting Information, Figures S1–S4.

The higher energy orbitals of π- and δ-character are found to mix significantly with the Cp*- and Am-orbitals, resulting in a further splitting of these orbital sets, which is particularly notable for the π*–π*–π* orbitals. The orbitals of **Mo/W^{therm}** appear to have more metal/ligand mixing than **Mo/W^{photo}**, which is presumably due to better overlap of metal and ligand orbitals. Due to mixing of ligand and core orbital character, there are two distinct sets of π*–π*–π* pairs in which the orbitals are energetically almost degenerate for both thermally active complexes; the higher energy set is greyed out in Figure 3b. While the degeneracy of these π*–π*–π* pairs is retained in **W^{photo}**, it is completely lifted in **Mo^{photo}**, resulting in a different energetic ordering of the unoccupied orbitals. Similarly, the unoccupied orbitals of predominant σ-character do not follow a clear trend across the series. The unoccupied δ/δ*-orbitals appear to be closer in energy in the photoactive complexes than in the thermally active complexes, which is presumably due to the differences in inductive effects of the Am ligands since all other components remain the same.

Analysis of Predicted Spectra with Molecular Orbital Scheme and Difference Densities

For **Mo^{photo}**, the UV/Vis spectrum predicted with the density functional LC-BLYP showed acceptable agreement with the experimental spectrum, albeit blue-shifted by ca. 0.98 eV.[16b] The envelopes of the spectra for the Mo complexes are very similar with high intensity features at ca. 4.6 and 5.3 eV, see Figure 4.

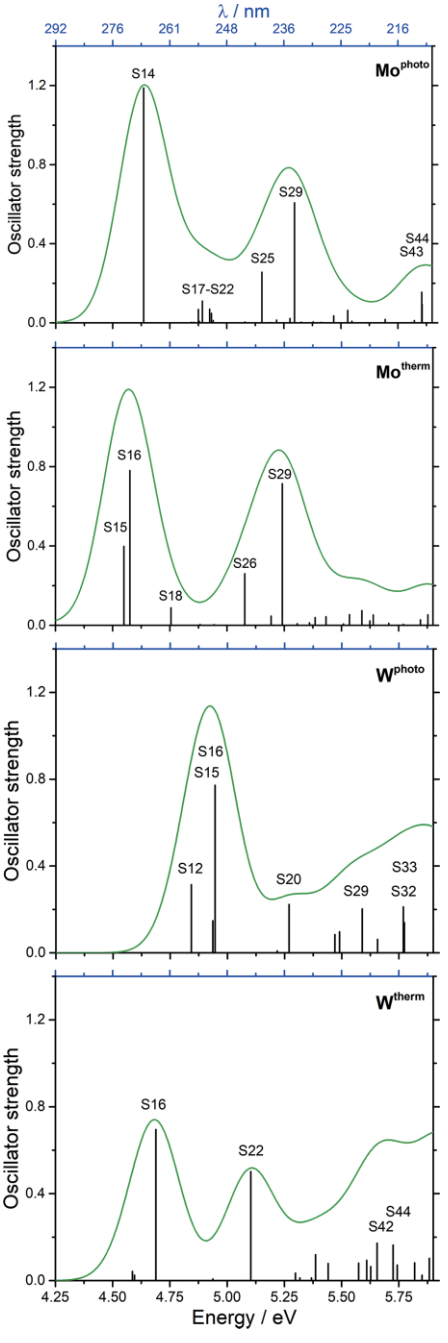

Figure 4. UV/Vis spectra predicted by TD-DFT with the density functional LC-BLYP for all complexes; from top to bottom: **Mo^{photo}**, **Mo^{therm}**, **W^{photo}**, **W^{therm}**; note that the energies were not shifted to match experiment. The line spectrum is broadened by 0.25 eV. The most intense transitions S_n are labelled; different types of analysis of selected transitions are discussed below (for remaining transitions, see Supporting Information, Table S2).

The predicted spectrum of **W^{therm}** has an overall lower intensity profile with peaks at 4.7 and 5.1 eV. The spectrum of **W^{photo}** is shifted to slightly higher energy with the highest intensity features at ca. 4.9 and 6.0 eV. The energy difference between the first high intensity features of **Mo^{photo}** and **W^{photo}** is consistent with that observed experimentally.[12e]

As the first tier of spectral analysis, the transitions are assigned based on the contributing molecular orbitals, see Table 2 for a few representative examples. Data for all labeled transitions are shown in the Supporting Information, Table S2, alongside the relevant MOs for all transitions, Figures S1–S4. We use MLCT and LMCT as abbreviations for metal-to-ligand charge transfer and ligand-to-metal charge transfer, respectively.

Table 2. Selected transitions S_n, labelled as in Figure 4, with their excitation energies E (eV), oscillator strengths f_{osc}, contributions C (%; C > 10 %) and character of donor and acceptor orbitals (see Figures S1–S4 for orbitals).

S_n E, f_{osc}	C	Don. Orbital	Acc. Orbital	S_n E, f_{osc}	C	Don. Orbital	Acc. Orbital
		Mo^{photo}				**Mo^{therm}**	
S_{14} *4.64, 0.10*	10	168 L_{Cp*}	175 π*-π-π*	**S_{15}** *4.55, 0.08*	11	187 ππ*π	191 π*-π-π*
	28	171 ππ*π	175 π*-π-π*		18	188 ππ*π	192 core/L_{Am}
	32	172 ππ*π	176 π*-π-π*				
S_{19} *4.89, 0.01*	20	169 L_{Cp*}	176 π*-π-π*	**S_{18}** *4.76, 0.02*	27	188 ππ*π	194 Mo-L_{Am}
	12	174 δ/δ*	186 σ*-σ-σ*		20	188 ππ*π	200 core/L_{Am}
S_{25} *5.15, 0.04*	44	171 ππ*π	177 core & L	**S_{26}** *5.08, 0.06*	20	184 Mo-L_{Cp*}	191 π*ππ*
					10	187 ππ*π	194 Mo-L_{Am}
S_{29} *5.30, 0.08*	45	172 ππ*π	180 Mo-L_{Cp*}	**S_{29}** *5.24, 0.13*	15	188 ππ*π	200 core/L_{Am}
	20	172 ππ*π	181 L_{Cp*}-L_{Am}		26	188 ππ*π	201 Mo-L_{Cp*}
					11	188 ππ*π	206 L_{Cp*}-L_{Am}
		W^{photo}				**W^{therm}**	
S_{12} *4.84, 0.04*	13	173 δ/δ*	180 W-L_{Cp*}	**S_{16}** *4.69, 0.17*	31	187 ππ*π	191 W-L_{Am}
	16	174 δ/δ*	183 W-L_{Cp*}		11	188 ππ*π	196 π*ππ*
	19	174 δ/δ*	187 σ*-σ-σ*				
S_{16} *4.95, 0.12*	18	171 ππ*π	176 π*-π-π*	**S_{22}** *5.10, 0.11*	18	188 ππ*π	196 π*ππ*
	28	172 ππ*π	175 π*-π-π*		18	189 δ/δ*	192 L_{Am}
					11	190 δ/δ*	191 W-L_{Am}
S_{20} *5.27, 0.03*	51	171 ππ*π	178 W-L_{Am}	**S_{42}** *5.66, 0.03*	17	189 δ/δ*	194 L_{Cp*}
					11	190 δ/δ*	202 W-L_{Cp*}
S_{32} *5.77, 0.05*	14	171 ππ*π	181 L_{Am}	**S_{44}** *5.73, 0.04*	22	188 ππ*π	195 π*ππ*
	32	172 ππ*π	181 L_{Am}		11	190 δ/δ*	202 W-L_{Cp*}

The transitions at 4.64 eV (S_{14}, **Mo^{photo}**) and 4.55/4.58 eV (S_{15}/S_{16}, **Mo^{therm}**) are predominantly due to excitations from π–π*–π orbitals into π*–π–π* orbitals. As discussed before,[16b] the cluster of transitions (S_{17}–S_{22}) predicted below 5 eV for **Mo^{photo}** does not have an equivalent in **Mo^{therm}**, where only one isolated transition is found at 4.75 eV (S_{18}). While for **Mo^{therm}**, the donor and acceptor orbitals are of π–π*–π and π–π*–π or δ/δ* character, respectively, the donor orbitals in **Mo^{photo}** are predominantly localized on various ligands and the acceptor orbitals are the two π*–π–π* orbitals (the only exception being transition S_{22}, see Table S2). The transitions at 5.15 eV (S_{25}, **Mo^{photo}**) and 5.08 eV (S_{26}, **Mo^{therm}**) are mostly due to excitations from π–π-*π to δ/δ* orbitals with significant Am-ligand character. At 5.30 eV (S_{29}, **Mo^{photo}**) and 5.25 eV (S_{29}, **Mo^{therm}**), the excitations originate from π–π*–π orbitals going into δ/δ* and Cp*/Am-centered orbitals.

In **W^{photo}**, the first intense transition, S_{12} at 4.84 eV, has several contributions characterized as excitations from δ/δ*-orbitals to orbitals that involve the metal and the directly attached Cp* ligand. The more than twice as intense transition S_{16} at 4.95 eV is due to excitations from π–π*–π orbitals into π*–π–π* orbitals, akin to the low-energy end of the molybdenum complexes. In the first intense transition of **W^{therm}** (S_{16}, 4.69 eV) the same character is found, albeit with more pronounced ligand character among the acceptor orbitals. At 5.10 eV, transition S_{22} of **W^{therm}** has several equally weighted contributions: π–π*–π to π*–π–π*, δ/δ* to an Am-based orbital, and δ/δ* to an orbital with tungsten and Am-ligand contributions. In the transition of **W^{photo}** at similar energy (5.27 eV), the dominant contributor is an excitation from a π–π*–π orbital to an orbital with mixed tungsten/Am character. We note, however, that this dominant contribution makes up only 51 % of the character of the transition, which is among the largest coefficients in the highest intensity excitations. The excitations predicted at higher energies for both tungsten complexes have π–π*–π and δ/δ* donor orbitals and acceptor orbitals of either pure ligand or mixed ligand-tungsten character.

In both the tungsten and the molybdenum complexes, charge-transfer character appears to be widely spread. As expected from the MO-scheme excitations from π–π*–π- and δ/δ*-orbitals into the low-lying unoccupied π*–π–π* and ligand orbitals are prevalent. However, neither a qualitative impression nor a quantitative evaluation of striking differences between the molybdenum and tungsten complexes, or the photoactive and thermally active species is possible based on these data.

From the above results, it becomes clear that an analysis based purely on the MOs is not only cumbersome, but also open to a significant degree of interpretation by the researcher. Difference densities, i.e. the difference between the excited state and ground state densities, offer a combined view of the various individual contributions to an excited state. Figure 5 shows the difference densities corresponding to the representative transitions of Table 2. Density depletions (yellow) and density gains (red) can be easily distinguished. They can also be assigned to the chemical subunits of the complexes, i.e. the M-N-N-M core, the Am or Cp* ligands. Of course, this may not be the case for more localized transitions, which are not shown here.

However, due to the way the information about the character of the transition and the individual contributors is compressed, it is not in all cases trivial to recognize the dominant contributing orbitals in the difference densities (e.g. transition S_{16} of **W^{therm}**). In other cases, the MO-based analysis might be fragmented to such an extent that it does not convey all rele-

Full Paper
doi.org/10.1002/ejic.201901304

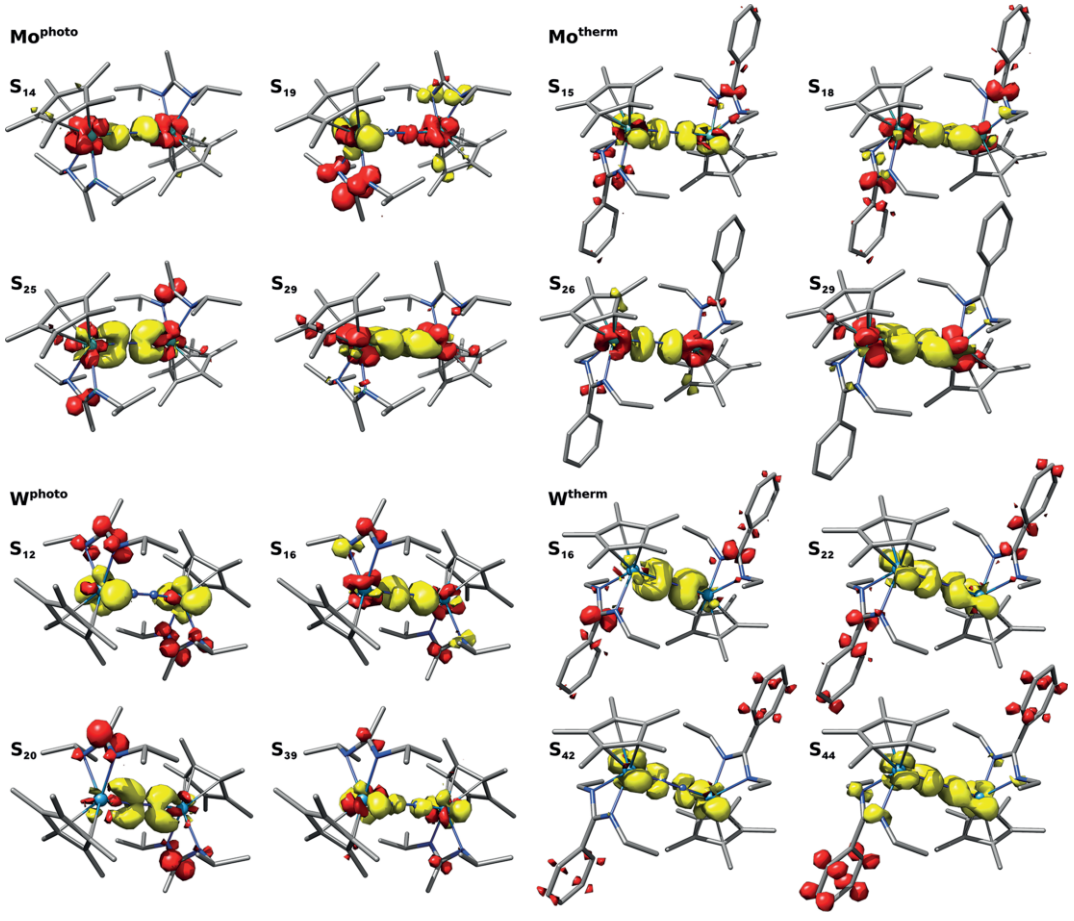

Figure 5. Difference densities of highest intensity transitions in **Mo^{photo}**, **Mo^{therm}**, **W^{photo}** and **W^{therm}** of the LC-BLYP-predicted spectra. Density loss is shown in yellow, density gains are shown in red. The contour value is 0.03.

vant contributions. For instance, the difference densities of states S_{29} of **Mo^{photo}** and **Mo^{therm}** show some contributions from the Am-ligands to the donor density; this is not apparent from the analysis of dominant MO contributors. This effect can be seen even more clearly in transition S_{16} of **W^{photo}**. We can conclude that an analysis of difference densities offers an advantage over a simple manual inspection of the orbitals but that it still does not allow any quantitative analysis or a satisfactory comparison of character between different chemical species.

Analysis of Predicted Spectra with TheoDORE

Owing to the fact that neither an inspection of the molecular orbitals nor an analysis of the difference densities proved sufficient to understand the excited states involved in these systems, we proceed to the third tier of our electronic structure analysis. For this purpose, we postprocess the TD-DFT results using the TheoDORE package.[1] TheoDORE aims at providing completely automated and, at the same time, rigorous routines for the analysis of excited-state computations. The implemented methods have been applied successfully for a variety of systems, such as interacting DNA bases,[25] conjugated polymers,[26] and transition metal complexes,[27] and recent work shows how this information can be used to gain insight into excitation energies beyond the MO picture.[28] Herein, we investigate whether this analysis approach is also advantageous for multinuclear transition metal complexes. We employ a fragment-based analysis scheme that allows an automated assignment of excited-state character. This method has been reviewed recently[29] and we shall only outline a few points here. The analysis within TheoDORE is based on the picture of a correlated electron-hole pair and one monitors on which part of the system the electron and hole, respectively, reside. For this purpose, the system is divided into different fragments and the so-called charge transfer numbers Ω_{AB}[1a,30] are computed between these fragments (see Figure 6). Here, Ω_{AB} denotes the probability that the hole is on a fragment *A* of the system while the electron is on *B*. A diagonal element Ω_{AA} gives the weight of a local excitation on fragment *A* while an off-diagonal Ω_{AB} represents charge transfer. The total Ω-matrix can be conveniently represented as a pseudocolour matrix plot[26,31] where the fragments of a molecule, i.e. individual atoms or groups of atoms, run along the rows and columns, see e.g. Figure 7. This representation is explored in the following.

Figure 6 shows how the analysis extends to a dinuclear transition metal complex. For this purpose, a model system is considered containing two metal centers (M1, M2), the bridging

Full Paper
doi.org/10.1002/ejic.201901304

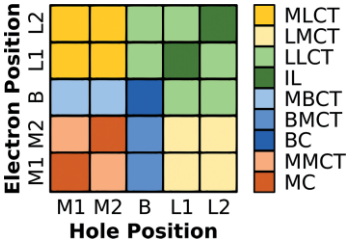

Figure 6. Illustration of the types of excitation quantified by TheoDORE in this contribution.[27,29] Nomenclature used is an extension of that used commonly in the literature; MC: metal-centered; MMCT: metal-to-metal charge transfer; BC: bridge-centered; BMCT: bridge-to-metal charge transfer; MBCT: metal-to-bridge charge transfer; IL: intra-ligand; LLCT: ligand-to-ligand charge transfer; LMCT: ligand-to-metal charge transfer; MLCT: metal-to-ligand charge transfer.

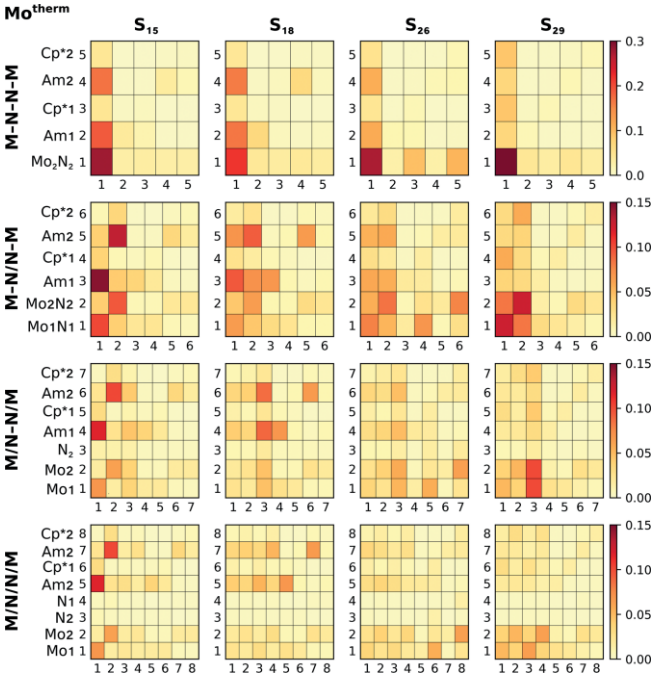

Figure 7. Ω-matrices for transitions S_{15}, S_{18}, S_{26} and S_{29} of the LC-BLYP-predicted spectrum of **Mo^{therm}** in all four fragmentation schemes. Labels on the rows and columns correspond to the same fragment; those on the columns refer to the hole, those on the rows to the electron.

unit (B, here: μ-N_2), and two ligands (L1, L2). Given five fragments, there are 25 different possibilities to place the electron and hole in one of them, and these can be assigned different meanings. If, for example, the hole and electron are both on M1, the state is characterized as metal-centered (MC), whereas if the hole is on M1 and the electron on a ligand, it would be characterized as a metal-to-ligand charge transfer (MLCT) state. The full set of categories is presented in Figure 6. Any given excited state will be a combination of these categories, the contributions of which are represented in a pseudocolor matrix plot. Note that this analysis exceeds the above-mentioned processes of analysing MO contributions or visualizing difference densities in two crucial ways. First, the information is completely quantitative and reproducible. Second, one can disentangle different overlapping excited state processes, e.g. two opposing CT states yielding no overall net transfer of charge.[1a]

The Sita complexes represent a well-suited, but at the same time challenging test case to study the application of the TheoDORE analysis tools to multinuclear transition metal complexes: on the one hand, they have singlet ground states so that a DFT description should be perfectly sufficient, and the lowest excitations will go into low-lying antibonding valence orbitals for which a good description is expected. On the other hand, as is well known and can be readily seen from the molecular orbitals, the bonding situation in the linear M-N-N-M units is highly covalent. Identifying a chemically sensible and useful fragmentation scheme for these complexes is thus not straightforward. Always taking each Am and Cp* ligands as individual fragments, four fragmentation schemes of the core are considered below: (i) M-N-N-M; (ii) M-N/N-M; (iii) M/N-N/M; (iv) M/N/N/M. Here, dash (slash) means that the two atoms are assigned to the same (different) fragment. Of these schemes, scheme (iii) corresponds to the decomposition shown in Figure 6, except that in the following four ligands are considered. We begin the discussion of fragmentation schemes and the corresponding Ω-matrices with high intensity transitions for **Mo^{therm}**. All Ω-matrices with the absolute values are provided as Supporting Information alongside all other descriptors delivered by TheoDORE; please note that the colour scales vary between fragmentation schemes.

In the fragmentation scheme M-N-N-M, where the entire core is taken as one fragment (Figure 7, first row), the first set of intense transitions (S_{15}, S_{16} (not shown in Figure 7)) in **Mo^{therm}** are local excitations within the core with some charge-transfer character from the core to the Am ligands. Transition S_{18} has additional contributions from excitations within the Am ligands. Transitions S_{26} and S_{29} are again dominated by local excitations within the M-N-N-M core with small CT contributions from and to the ligands. A more detailed insight into these excited states can be gleaned by fragmenting the core according to the M-N/N-M and M/N-N/M patterns (Figure 7, second and third row). From these fragmentation schemes the charge transfer character in the lowest energy transitions S_{15} and S_{16} is found to originate from each molybdenum ion going into the directly bound Am ligands. In contrast, the CT to the Am ligands in transition S_{18} appears to come dominantly from the N_2 bridge. Transition S_{26} can be most clearly analyzed in the M/N-N/M fragmentation scheme: there are BMCT/LMCT contributions are from N_2 unit and the Cp* ligands to the molybdenum ions, and the LLCT contributions originate from the N_2 bridge going into the Am ligands. The characterization of transition S_{29} is reflected differently in the M-N/N-M and M/N-N/M fragmentation schemes where in the former local excitations within the M-N units dominate and in the latter charge transfer from the N_2-bridge to the metal ions appears. These different, but equally valid interpretations are reflective of the high degree of covalency in the Mo_2N_2 core.

Further fragmenting the central M_2N_2 core into the individual atoms does not provide any additional insight (see Figure 7, last row). One can rather notice that the information is diluted or even lost: the hole is apparently rather delocalized over the

M-N-N-M unit so that hole and electron cannot be spotted immediately in the more fragmented representation.

The first important transition in **W^{therm}**, S_{16}, is of similar character as S_{18} in **Mo^{therm}**, i.e. dominated by local excitations within the M-N-N-M unit and MLCT to the Am ligands, see Figure 8. Upon closer inspection in fragmentation scheme (iii) they are revealed as N_2 bridge to tungsten charge transfer transitions, alongside CT contributions from the N_2 bridge to the Am ligands. Transition S_{22} is instead dominated by CT from the tungsten ions to the Am ligands. At higher energies, transitions S_{42} and S_{44} are characterized by MLCT to the Cp* and Am ligands as well as local excitations involving the two Cp* and Am ligands themselves. Overall, a difference between the thermally active Mo and W complexes appears to be that the MLCT in **W^{therm}** is more well-defined while it seems somewhat more spread in **Mo^{therm}**, and that the LMCT contributions are stronger in **Mo^{therm}** than in **W^{therm}**.

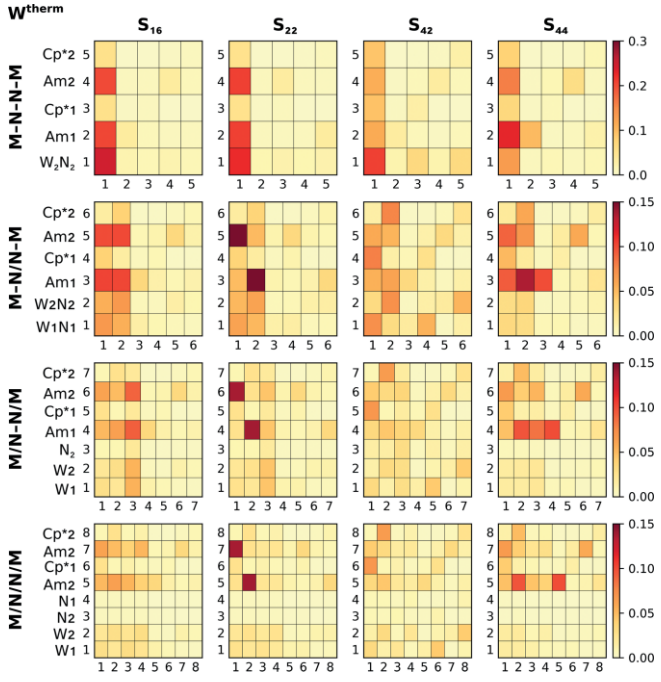

Figure 8. Ω-matrices for transitions S_{16}, S_{22}, S_{42} and S_{44} of the LC-BLYP-predicted spectrum of **W^{therm}** in all four fragmentation schemes. Labels on the rows and columns correspond to the same fragment; those on the columns refer to the hole, those on the rows to the electron.

Unlike for the previously discussed thermally active complexes, many of the high-intensity transitions of the photoactive tungsten dimer **W^{photo}** involve more simultaneous charge transfer excitations from and to both types of ligand, see Figure 9. Transition S_{12}, for instance, is due to excitations from tungsten to the directly bound Am and Cp* ligands. Transition S_{15} is characterized by local excitations on the Am ligands as well as LMCT from the Am to the tungsten ions (see Supporting Information). The highest intensity transition S_{16} is characterized by local excitations in the M-N units of the M-N/N-M fragmentation scheme or rather LMCT from the N_2 bridge to the metals in the M/N-N/M fragmentation scheme reminiscent of transition S_{29} in **Mo^{therm}**. In particular in fragmentation scheme (ii), LMCT and MLCT contributions from and to both ligand types can be seen. Transition S_{20} appears to involve charge transfer from the N_2 bridge to the Am ligands, as can be clearly seen in the M/N-N/M fragmentation scheme. The remaining higher energy transitions are more similar in character to those of the thermally active species: they dominantly involve LMCT from Cp* to tungsten (S_{29}), and MLCT from tungsten to Cp* coupled to LMCT within the core (S_{32} and S_{33}).

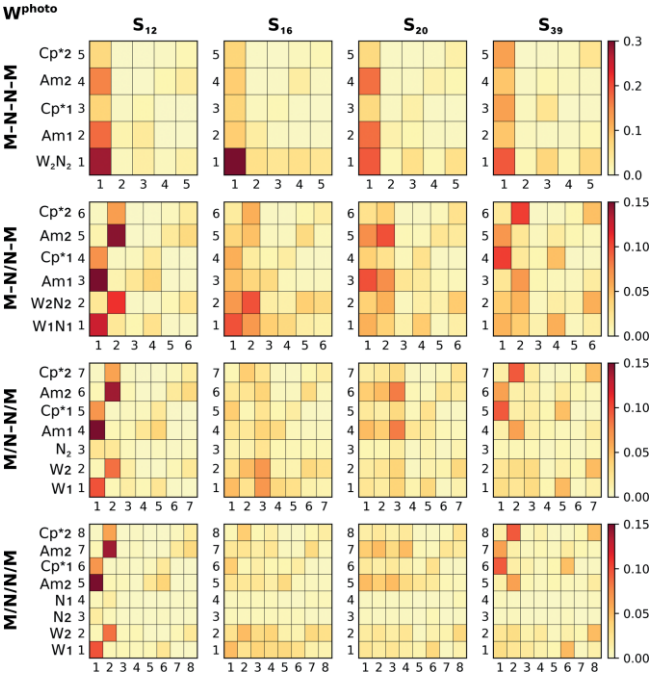

Figure 9. Ω-matrices for transitions S_{12}, S_{16}, S_{20} and S_{39} of the LC-BLYP-predicted spectrum of **W^{photo}** in all four fragmentation schemes. Labels on the rows and columns correspond to the same fragment; those on the columns refer to the hole, those on the rows to the electron.

For the photochemically active molybdenum dimer **Mo^{photo}**, Figure 10, the most intense transition S_{14} is characterized by local excitations within the MN fragments and LMCT from the Am ligands to the core. In contrast to S_{15} or S_{29} in **Mo^{therm}**, this state contains LMCT, not MLCT, of almost equal importance to these intra-core excitations. The other high intensity transitions S_{25} and S_{29} are of similar character, although with more pronounced MLCT character. In the cluster of low intensity transitions that appears to be quite unique to **Mo^{photo}**, S_{17}–S_{22}, all but transition S_{22} show various types and degrees of charge transfer: LMCT for S_{17}, S_{20} and S_{21}, MLCT for S_{18} and S_{19}. Transition S_{22} is closer in character to transition S_{16} in **W^{photo}** and S_{29} in **Mo^{therm}**, with N_2-bridge to metal CT or local excitations within MN fragments. As noted previously,[16b] these transitions show a high degree of asymmetry, which is quite obvious upon inspection of their Ω-matrices. Transition S_{17} can be assigned as LMCT from Am1 and Cp*1 to Mo1, transition S_{19} has the same type of local LMCT from Am2 and Cp*2 to Mo2 with additional MLCT from Mo1 to Am1, and MLCT between Mo1 and Am1, respectively. Similarly, transitions S_{20} and S_{21} are due to LMCT from Am1 and Cp*1 to Mo1, and from Am2 and Cp*2 to Mo2.

An overview of the state character and relative importance of local and CT excitations is given in a second representation

Full Paper
doi.org/10.1002/ejic.201901304

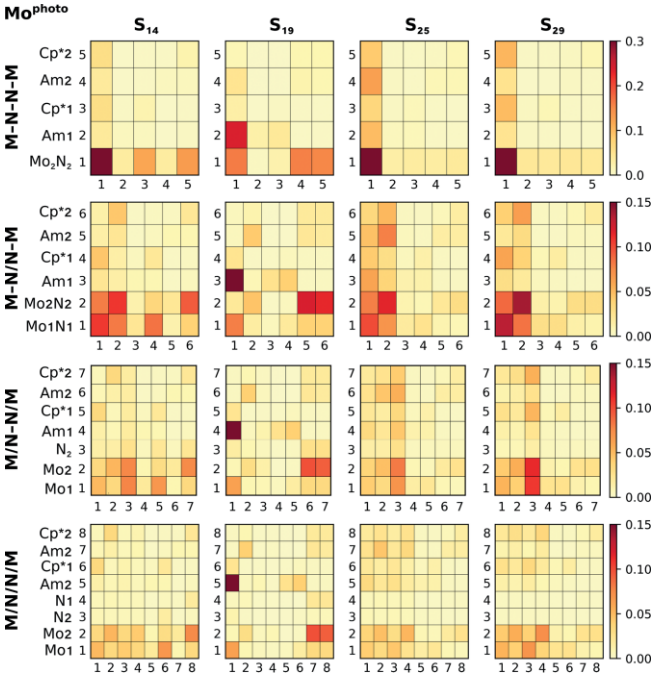

Figure 10. Ω-matrices for transitions S_{14}, S_{19}, S_{25} and S_{29} of the LC-BLYP-predicted spectrum of **Mo^{photo}** in all four fragmentation schemes. Labels on the rows and columns correspond to the same fragment; those on the columns refer to the hole, those on the rows to the electron.

accessible through TheoDORE. In Figure 11, we show in the lower panels the state character in terms of local excitations within the MN1 and MN2 fragments (dark blue), excitations between the MN_i fragments (light blue), MLCT as the sums of all Ω-matrix elements directly above the MN1 and MN2 fragments (red), and LMCT as the sums of all Ω-matrix elements to the right of the MN1 and MN2 fragments (orange). The energy (black steps) and oscillator strengths (colored bars) are indicated in the upper panels of Figure 8a-d. From this representation, it can be seen that the lowest states, S_1–S_{13}, are broadly similar for the molybdenum complexes. For the following transitions up to S_{21}, LMCT is more prominent in **Mo^{photo}**, while in the next transitions up to S_{25}, MLCT dominates. A parallel pattern is seen for the tungsten complexes: the transitions up to S_{11} are quite similar, whereas in the transitions roughly up to S_{30}, LMCT is more predominant in **W^{photo}** than in **W^{therm}**.

A Brief Comment on the Choice of Density Functional

It is well established that the energetic position of states with charge-transfer character is not predicted correctly with TD-DFT due to the asymptotic behavior of commonly used density functionals.[32] GGA, meta-GGA, and, to a lesser extent, hybrid functionals, tend to underestimate the energy of CT states by up to several eV. This behavior can be traced back to an incorrect, too quickly decaying description of the exchange-correlation potential at large distances from the nuclei, or in other words an improper description of large electron–hole separations.[33] The amount of Hartree–Fock-exchange in the density

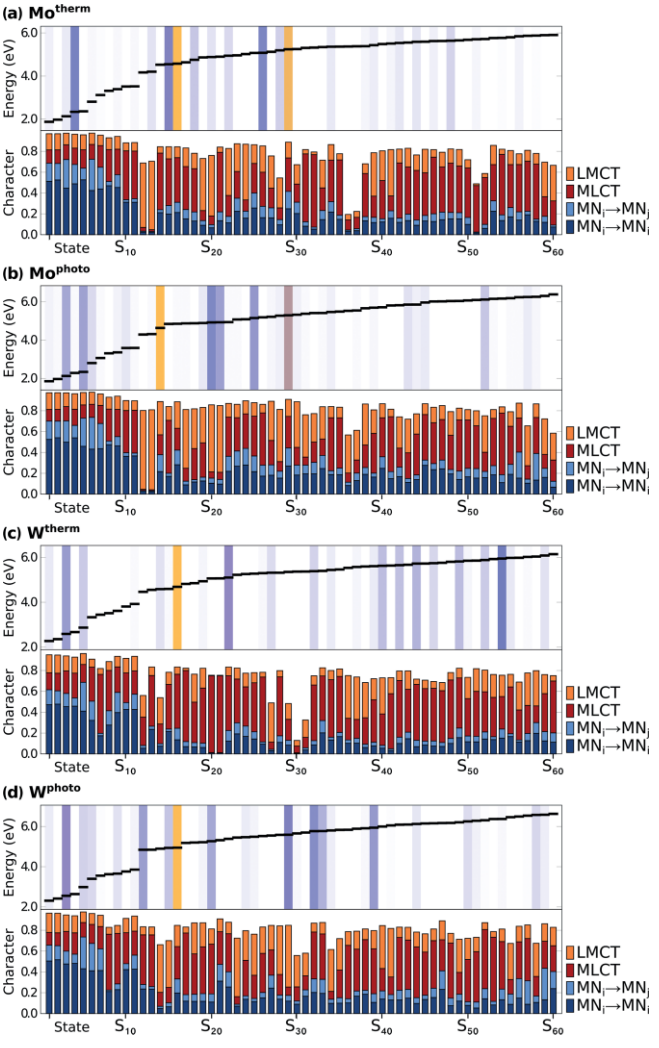

Figure 11. Character of states S_1–S_{60} for (a) **Mo^{therm}**, (b) **Mo^{photo}**, (c) **W^{therm}**, (b) **W^{photo}** based on the fragmentation scheme M-N/N-M. Each upper panel shows the oscillator strength as coloured bars (yellow: most intense, shades of blue: less intense) and the energy in eV as a step function.

functional strongly influences the energy of CT states because the exact exchange fraction shows better asymptotic behavior. A more fundamental correction of the asymptotic potential, in functionals known as long-range corrected or asymptotically corrected functionals (e.g. CAM-B3LYP,[34] LC-BLYP[35]), was shown to be effective. Excellent papers highlighting the theoretical background of charge-transfer description with TD-DFT and recent applications in particular for transition metal complexes are available in the literature.[32c,33b,33c,36]

Previous studies showed that both energies and state characters are strongly affected by the functional in organic molecules,[36c] conjugated polymers,[37] and mononuclear transition metal complexes,[27,38] and we want to assess this effect in the highly covalent multinuclear systems here. Using the state character representation provided by TheoDORE, we can evaluate whether transitions simply shift in energy or are also subject to change in character. The density functionals BLYP and B3LYP are chosen as representative examples, see Figure 12. The upper panels reveal that the intensity distribution depends dra-

matically on the functional, as expected. Taking the LC-BLYP data as reference values (lowest panel), the computations with BLYP appear to underestimate the the locally excited character within MN_i fragments, in particular for the lower energy excitations. This is overcompensated for with MLCT character (dark red). The calculations with B3LYP appear to better approximate the ratio of MLCT and LMCT, but also underestimate the contributions from excitations within and between MN fragments. Another observation that can be made for both complexes across the three functionals is that states characterized as dominantly LMCT in character (mostly orange in the lower panels) are predicted at very different energies.

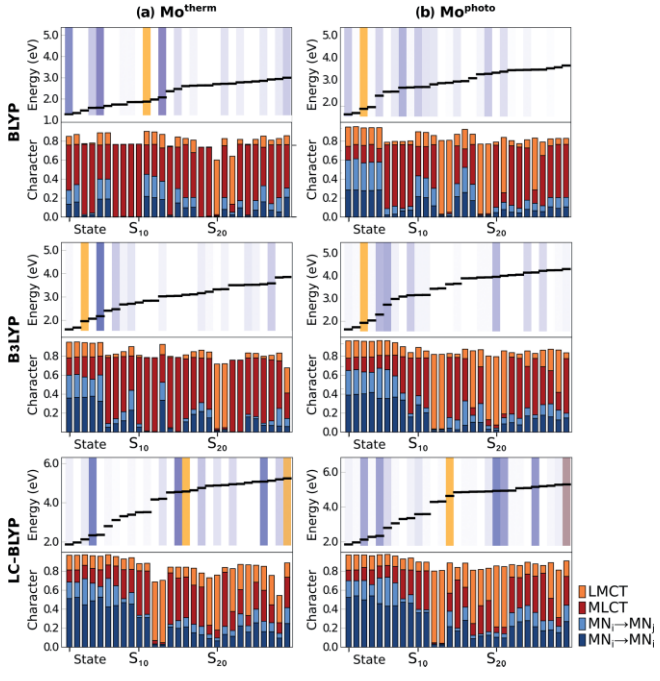

Figure 12. State character of states S_1–S_{29} according to BLYP (top), B3LYP (middle) and LC-BLYP (bottom) calculations for **Mo^{therm}** (a, left) and **Mo^{photo}** (b, right), based on the fragmentation scheme M-N/N-M.

Discussion

It is not surprising to find similar behavior for the complexes studied in this paper, as molybdenum and tungsten are generally known to have very similar chemistries and properties (e.g. atomic and ionic radii, electronegativities, standard potentials) due to the lanthanoid contraction. The main contributor for the observed thermal vs. photochemical reactivity must therefore stem from the ligand sphere. The thermal pathway will be feasible or obstructed depending on the accessibility of intermediates, i.e. the energetic barrier associated with the transition structures along the isomerization path. In order to follow the photochemical path, it appears plausible that some electronic structure criteria must be met to initiate the photoreaction; although here, too, an argument about internal conversion and intersystem crossing rates, energetic barriers along the photochemical path and the relative stability of intermediates can be made. Since we are currently not in a position to explore the full chemical space after photoexcitation, we have to restrict ourselves here to the initial step, i.e. the character of the relevant electronically excited states in the Franck–Condon region, and discuss which excited state(s) could plausibly initiate nitrogen photosplitting.

From the experimental paper, we recall that both **Mo^{photo}** and **W^{photo}** are thermally robust, and that the full photoconversion of the tungsten complex took significantly longer than for the molybdenum complex (72 h vs. 48 h, monitored by NMR).[12e] There is also experimental evidence in the form of isosbestic points that no intermediates were detected during the conversion of **W^{photo}**. In contrast, no isosbestic points were found for **Mo^{photo}**, indicative of intermediates that can be detected by UV/Vis. In the case of **Mo^{photo}**, the μ-N and bis-μ-N-bridged products were isolated and crystallographically characterized directly from the reaction mixture, thus providing at least one explanation for the absence of isosbestic points.

The irradiation was conducted with a Rayonet carousel of medium-pressure Hg lamps (RP$R\bar{3}$500A lamp),[12e] which emits at most between 280–420 nm with maximum emission around 350 nm (in eV: 2.95–4.43, max. 3.54; in cm^{-1}: 23810–35714, max: 36440). Considering that the TD-DFT-predicted spectra are blue-shifted by ca. 0.98 eV (7869 cm^{-1}),[16b] this implies that states S_{14}–S_{29} may be photoactive. This is precisely the region in which the LMCT-dominated transitions are found for **Mo^{photo}**, and in which appreciable LMCT character can also be found for **W^{photo}**. In agreement with the experimental observation of longer irradiation times for the tungsten complex, the intensities of the LMCT states in **W^{photo}** are generally lower.

A number of transitions with LMCT character can be found for **Mo^{therm}**, but they have vanishingly low intensities (S_{19}, S_{20}, S_{22}, S_{24}, see Figure 11), and in **W^{therm}** only S_{14} and S_{27} have significant LMCT character, again with near-vanishing intensity. Our analysis thus lends further support to Sita's previous suggestion[16a] that a viable mechanism for N_2 photoactivation in these complexes may involve LMCT excitations that could lead to partial ligand detachment or other structural distortions. Transferring an electron onto the M_2N_2 unit, as one formally would with an LMCT transition, is of course consistent with a reduction event that is required for nitrogen activation.

Several caveats of this analysis should be mentioned for completeness. Firstly, which excitation(s) are actually active can only be determined experimentally; it may well be that a particular type of charge redistribution within the M_2N_2 core, such as N_2-to-metal charge transfer (e.g. S_{16} in **W^{photo}**, S_{29} in **Mo^{photo}**), is responsible for inducing N_2 photosplitting. Secondly, at this point it cannot even be excluded that **Mo^{photo}** and **W^{photo}** follow different reaction paths, one indicator for different routes possibly being given by the fact that isosbestic points were only observed for **W^{photo}**. Finally, we would like to emphasize that other complexes capable of nitrogen photoactivation or -splitting may operate under completely different mechanisms, e.g. those introduced in Figure 1.[2,12f]

The electronic structure design for a complex capable of N_2 photosplitting via a LMCT mechanism should consider under which circumstances LMCT transitions become energetically favourable *and* gain sufficient intensity to become relevant.

Full Paper
doi.org/10.1002/ejic.201901304

Applying this design idea retroactively to the two different Am ligand spheres –(N(*i*Pr)C(Me)N(*i*Pr))⁻ in the photoactive, (N(Et)C(Ph)N(Et))⁻ in the thermally active complexes – it is however not obvious from common chemical concepts that one be more susceptible to LMCT excitations. This shows again that computational analyses, e.g. on the basis of TheoDORE, are a of high value to gain complementary insights to experimental observations.

Conclusions

A recurring problem in the analysis of TD-DFT-computed spectra is that many individual orbitals make small contributions to the predicted transitions. In such cases, an analysis based purely on the contributing orbitals may fall short. Difference densities can help in assigning such complicated spectra, however a quantitative evaluation of the characteristics of a transition is not possible. In this contribution, we applied the wavefunction analysis tools provided by TheoDORE to study the electronic structures of N_2-bridged molybdenum and tungsten complexes to obtain a detailed understanding on how variations in the ligand substitution pattern lead to differences in electronic excited states. Four complexes were studied: two dimers capable of thermal and two dimers capable of photochemical N_2 activation, each set with one molybdenum and one tungsten complex (**Mo^{therm}**, **Mo^{photo}**, **W^{therm}**, **W^{photo}**). These have highly covalent bonds in the central [M(μ-η^1:η^1-N_2)M] unit and thus the choice of fragmentation scheme is not obvious. From our results, it appears advisable to try several fragmentation schemes for systems that show high degrees of covalency and compare the outcomes, as different types of transition are reflected differently in the possible fragmentation schemes. In the present case, dividing the central M_2N_2 unit into either two metal-nitrido-like units or two metals and the N_2-bridge appears to reveal the relevant characteristics most readily.

In all complexes, significant charge transfer character is present in almost all high intensity transitions. This finding explains why LC-BLYP, a range-separated functional, was found to best reproduce the overall shape of the experimental spectrum of the photochemically active molybdenum dimer.[16b]

Although the requirements, mechanisms, energy scales and timescales of nitrogen photoactivation for these and most other complexes are presently unclear, a suggestion[16a] made for the systems studied here was that the N_2-cleaving step may involve a partial detachment of a supporting ligand. This is supported by the fact that more and higher intensity states with LMCT character were found in both photoactive complexes in the Franck–Condon region. Clearly, experimental and computational studies of the photophysical and photochemical processes after light excitation are needed to confirm the character of photoactive states and explore the reaction paths. If the scenario of LMCT-induced nitrogen photosplitting is confirmed, the design of ligand spheres that enable such transitions should consider how they can be enhanced in intensity and shifted to favorable energies.

Computational Details

All geometries were optimized with the same approach as previously,[16b] using the ORCA program package.[39] The crystal structures of **Mo^{therm}**,[16a] **W^{therm}**[16a] and **W^{photo}**[14b] were available in the literature as starting structures for the geometry optimisations. The BP86 density functional with the resolution of the identity approximation and an increased grid size (7 in ORCA nomenclature) and integration accuracy (7.0 in ORCA nomenclature) was used.[40] For W, Mo and N, the def2-TZVP basis set was, including the def2-ECP effective core potential for the metals; for C and H, the basis set def2-SVP was used.[41] As the auxiliary basis, def2/J was chosen.[42] The SCF and optimisation convergence criteria were set to "tight". Solvation and dispersion effects were considered through CPCM (benzene, ε = 2.28) and Grimme's atom-pairwise correction with Becke–Johnson-damping (D3BJ).[43] The TD-DFT calculations under consideration of the Tamm–Dancoff-approximation used the LC-BLYP functional with identical settings as for the geometry optimisations except for the solvation correction, where methyl cyclohexane (ε = 2.071) was chosen.[35,40c,44] This choice of functional was motivated by the good agreement with the experimental spectrum of **Mo^{photo}**, although the energy is shifted by ca. 0.98 eV. Additional RI-BLYP and RIJCOSX-B3LYP calculations were run to assess the dependence of the state composition on the density functional.[45] For all spectra, 60 roots were calculated, and the expansion space was chosen as five times as large. To obtain line spectra, the individual transitions were broadened with 0.25 eV.

For the TheoDORE analyses, the complexes were subjected to several fragmentation schemes as specified in the main text. For each complex in each fragmentation scheme, the routines *analyse_tden.py* and *plot_OmFrag.py* were run to obtain the Ω-matrices and their pictorial representations. The Ω descriptors for transition metal complexes were chosen. For the analysis of state character in the fragmentation scheme M-N/N-M, the routine *plot_Om_bars.py* was used, summing the entries of the Ω-matrices according to the following hole/electron indices: $MN_i \rightarrow MN_i$ (1 1, 2 2), $MN_i \rightarrow MN_j$ (1 2, 2 1); MLCT (1 3, 1 4, 1 5, 1 6, 2 3, 2 4, 2 5, 2 6); LMCT (6 1, 5 1, 4 1, 3 1, 6 2, 5 2, 4 2, 3 2). We note here that the difference between the height of the bar and 1 is due to hole/electron pairs not considered, e.g. LLCT contributions such as (6 6, 5 3).

Acknowledgments

Computing time at the Balena High Performance Computing (HPC) Service at the University of Bath and the Lichtenberg high performance computer of TU Darmstadt are gratefully acknowledged.

Keywords: Nitrogen activation · Electronic structure · Molybdenum · Tungsten · Density functional theory calculations

[1] a) F. Plasser, H. Lischka, *J. Chem. Theory Comput.* **2012**, *8*, 2777–2789; b) F. Plasser, M. Wormit, A. Dreuw, *J. Chem. Phys.* **2014**, *141*, 024106.
[2] V. Krewald, *Dalton Trans.* **2018**, *47*, 10320–10329.
[3] J. G. Chen, R. M. Crooks, L. C. Seefeldt, K. L. Bren, R. Morris Bullock, M. Y. Darensbourg, P. L. Holland, B. Hoffman, M. J. Janik, A. K. Jones, M. G. Kanatzidis, P. King, K. M. Lancaster, S. V. Lymar, P. Pfromm, W. F. Schneider, R. R. Schrock, *Science* **2018**, *360*, eaar6611.
[4] a) J. K. Kowalska, J. T. Henthorn, C. Van Stappen, C. Trncik, O. Einsle, D. Keavney, S. DeBeer, *Angew. Chem. Int. Ed.* **2019**, *58*, 9373–9377; b) D. Sippel, M. Rohde, J. Netzer, C. Trncik, J. Gies, K. Grunau, I. Djurdjevic, L. Decamps, S. L. A. Andrade, O. Einsle, *Science* **2018**, *359*, 1484–1489; c) S. Rafiq, M. J. Bezdek, P. J. Chirik, G. D. Scholes, *Chem* **2019**, *5*, 402–416; d) C. Van Stappen, R. Davydov, Z. Y. Yang, R. Fan, Y. Guo, E. Bill, L. C. Seefeldt, B. M. Hoffman, S. DeBeer, *Inorg. Chem.* **2019**, *58*, 12365–12376.
[5] a) C. Köthe, C. Limberg, *Z. Anorg. Allg. Chem.* **2015**, *641*, 18–30; b) Y. Roux, C. Duboc, M. Gennari, *ChemPhysChem* **2017**, *18*, 2606–2617; c) S. C. Stieber, C. Milsmann, J. M. Hoyt, Z. R. Turner, K. D. Finkelstein, K. Wieghardt, S. DeBeer, P. J. Chirik, *Inorg. Chem.* **2012**, *51*, 3770–3785; d) R. J. Burford, A. Yeo, M. D. Fryzuk, *Coord. Chem. Rev.* **2017**, *334*, 84–99; e) S. M. Bhutto, P. L. Holland, *Eur. J. Inorg. Chem.* **2019**, 2019, 1861–1869; f) A. Simonneau, M. Etienne, *Chem. Eur. J.* **2018**, *24*, 12458–12463; g) A. J. Ruddy, D. M. C. Ould, P. D. Newman, R. L. Melen, *Dalton Trans.* **2018**, *47*, 10377–10381; h) K. Arashiba, A. Eizawa, H. Tanaka, K. Nakajima, K. Yoshizawa, Y. Nishibayashi, *Bull. Chem. Soc. Jpn.* **2017**, *90*, 1111–1118.
[6] a) N. Khoenkhoen, B. de Bruin, J. N. H. Reek, W. I. Dzik, *Eur. J. Inorg. Chem.* **2015**, *2015*, 567–598; b) M. H. Vu, M. Sakar, S. A. Hassanzadeh-Tabrizi, T. O. Do, *Adv. Mater. Interfaces* **2019**, *6*, 1900091; c) S. Kuriyama, Y. Nishibayashi, in *Nitrogen Fixation, Vol. 60* (Ed.: Y. Nishibayashi), Springer, Cham, **2017**, pp. 215–234; d) N. Stucke, B. M. Flöser, T. Weyrich, F. Tuczek, *Eur. J. Inorg. Chem.* **2018**, 2018, 1337–1355; e) Y. Ashida, K. Arashiba, K. Nakajima, Y. Nishibayashi, *Nature* **2019**, *568*, 536–540.
[7] a) F. Studt, F. Tuczek, *J. Comput. Chem.* **2006**, *27*, 1278–1291; b) M. Holscher, W. Leitner, *Chem. Eur. J.* **2017**, *23*, 11992–12003; c) H. Tanaka, K. Yoshizawa, in *Nitrogen Fixation, Vol. 60* (Ed.: Y. Nishibayashi), Springer, Cham, **2017**, pp. 171–196.
[8] a) N. Hazari, *Chem. Soc. Rev.* **2010**, *39*, 4044–4056; b) J. L. Crossland, D. R. Tyler, *Coord. Chem. Rev.* **2010**, *254*, 1883–1894; c) K. C. MacLeod, S. F. McWilliams, B. Q. Mercado, P. L. Holland, *Chem. Sci.* **2016**, *7*, 5736–5746.
[9] a) J. M. Smith, in *Progress in Inorganic Chemistry Volume 58*, John Wiley & Sons, Inc. **2014**, pp. 417–470; b) W.-L. Man, W. W. Y. Lam, T.-C. Lau, *Acc. Chem. Res.* **2014**, *47*, 427–439.
[10] D. Wang, F. Loose, P. J. Chirik, R. R. Knowles, *J. Am. Chem. Soc.* **2019**, *141*, 4795–4799.
[11] I. Klopsch, E. Y. Yuzik-Klimova, S. Schneider, in *Nitrogen Fixation, Vol. 60* (Ed.: Y. Nishibayashi), Springer, Cham, **2017**, pp. 71–112.
[12] a) E. Solari, C. Da Silva, B. Iacono, J. Hesschenbrouck, C. Rizzoli, R. Scopelliti, C. Floriani, *Angew. Chem. Int. Ed.* **2001**, *40*, 3907–3909; *Angew. Chem.* **2001**, *113*, 4025; b) J. J. Curley, T. R. Cook, S. Y. Reece, P. Müller, C. C. Cummins, *J. Am. Chem. Soc.* **2008**, *130*, 9394–9405; c) H. Kunkely, A. Vogler, *Angew. Chem. Int. Ed.* **2010**, *49*, 1591–1593; *Angew. Chem.* **2010**, *122*, 1636; d) T. Miyazaki, H. Tanaka, Y. Tanabe, M. Yuki, K. Nakajima, K. Yoshizawa, Y. Nishibayashi, *Angew. Chem. Int. Ed.* **2014**, *53*, 11488–11492; *Angew. Chem.* **2014**, *126*, 11672; e) A. J. Keane, W. S. Farrell, B. L. Yonke, P. Y. Zavalij, L. R. Sita, *Angew. Chem. Int. Ed.* **2015**, *54*, 10220–10224; *Angew. Chem.* **2015**, *127*, 10358; f) F. Schendzielorz, M. Finger, J. Abbenseth, C. Würtele, V. Krewald, S. Schneider, *Angew. Chem. Int. Ed.* **2019**, *58*, 830–834; *Angew. Chem.* **2019**, *131*, 840–844; g) Q. J. Bruch, G. P. Connor, C.-H. Chen, P. L. Holland, J. M. Mayer, F. Hasanayn, A. J. M. Miller, *J. Am. Chem. Soc.* **2019**, *141*, 20198–20208.
[13] a) C. Mao, J. Wang, Y. Zou, H. Li, G. Zhan, J. Li, J. Zhao, L. Zhang, *Green Chem.* **2019**, *21*, 2852–2867; b) R. Li, *Chin. J. Catal.* **2018**, *39*, 1180–1188.
[14] a) D. Sellmann, A. Hille, A. Rosler, F. W. Heinemann, M. Moll, G. Brehm, S. Schneider, M. Reiher, B. A. Hess, W. Bauer, *Chem. Eur. J.* **2004**, *10*, 819–830; b) P. P. Fontaine, B. L. Yonke, P. Y. Zavalij, L. R. Sita, *J. Am. Chem. Soc.* **2010**, *132*, 12273–12285; c) G. A. Silantyev, M. Förster, B. Schluschaß, J. Abbenseth, C. Würtele, C. Volkmann, M. C. Holthausen, S. Schneider, *Angew. Chem. Int. Ed.* **2017**, *56*, 5872–5876; *Angew. Chem.* **2017**, *129*, 5966; d) A. Eizawa, Y. Nishibayashi, in *Nitrogen Fixation, Vol. 60* (Ed.: Y. Nishibayashi), Springer, Cham, **2017**, pp. 153–169; e) B. M. Lindley, R. S. Van Alten, M. Finger, F. Schendzielorz, C. Würtele, A. J. M. Miller, I. Siewert, S. Schneider, *J. Am. Chem. Soc.* **2018**, *140*, 7922–7935.
[15] A. S. Huss, J. J. Curley, C. C. Cummins, D. A. Blank, *J. Phys. Chem. B* **2013**, *117*, 1429–1436.
[16] a) L. M. Duman, W. S. Farrell, P. Y. Zavalij, L. R. Sita, *J. Am. Chem. Soc.* **2016**, *138*, 14856–14859; b) V. Krewald, *Front. Chem.* **2019**, *7*, 352.
[17] S. Rafiq, M. J. Bezdek, M. Koch, P. J. Chirik, G. D. Scholes, *J. Am. Chem. Soc.* **2018**, *140*, 6298–6307.
[18] a) M. Reiher, B. Kirchner, J. Hutter, D. Sellmann, B. A. Hess, *Chem. Eur. J.* **2004**, *10*, 4443–4453; b) V. Krewald, L. González, *Chem. Eur. J.* **2018**, *24*, 5112–5123.
[19] a) M. C. Heitz, K. Finger, C. Daniel, *Coord. Chem. Rev.* **1997**, *159*, 171–193; b) M. Richter, P. Marquetand, J. González-Vázquez, I. Sola, L. González, *J. Chem. Theory Comput.* **2011**, *7*, 1253–1258; c) J. Eng, C. Gourlaouen, E. Gindensperger, C. Daniel, *Acc. Chem. Res.* **2015**, *48*, 809–817; d) M. Chergui, *Acc. Chem. Res.* **2015**, *48*, 801–808; e) S. Mai, P. Marquetand, L. González, *Int. J. Quantum Chem.* **2015**, *115*, 1215–1231; f) R. Monni, G. Capano, G. Aubock, H. B. Gray, A. Vlcek, I. Tavernelli, M. Chergui, *Proc. Natl. Acad. Sci. USA* **2018**, *115*, E6396–E6403.
[20] M. Hirotsu, P. P. Fontaine, P. Y. Zavalij, L. R. Sita, *J. Am. Chem. Soc.* **2007**, *129*, 12690–12692.
[21] A. J. Keane, B. L. Yonke, M. Hirotsu, P. Y. Zavalij, L. R. Sita, *J. Am. Chem. Soc.* **2014**, *136*, 9906–9909.
[22] a) M. Hirotsu, P. P. Fontaine, A. Epshteyn, P. Y. Zavalij, L. R. Sita, *J. Am. Chem. Soc.* **2007**, *129*, 9284–9285; b) B. L. Yonke, A. J. Keane, P. Y. Zavalij, L. R. Sita, *Organometallics* **2011**, *31*, 345–355.
[23] a) J. P. Reeds, B. L. Yonke, P. Y. Zavalij, L. R. Sita, *J. Am. Chem. Soc.* **2011**, *133*, 18602–18605; b) B. L. Yonke, J. P. Reeds, P. Y. Zavalij, L. R. Sita, *Angew. Chem. Int. Ed.* **2011**, *50*, 12342–12346; *Angew. Chem.* **2011**, *123*, 12550; c) L. M. Duman, L. R. Sita, *J. Am. Chem. Soc.* **2017**, *139*, 17241–17244.
[24] a) I. M. Treitel, M. T. Flood, R. E. Marsh, H. B. Gray, *J. Am. Chem. Soc.* **1969**, *91*, 6512–6513; b) D. E. Richardson, J. P. Sen, J. D. Buhr, H. Taube, *Inorg. Chem.* **1982**, *21*, 3136–3140.
[25] J. J. Nogueira, F. Plasser, L. González, *Chem. Sci.* **2017**, *8*, 5682–5691.
[26] S. A. Mewes, J.-M. Mewes, A. Dreuw, F. Plasser, *Phys. Chem. Chem. Phys.* **2016**, *18*, 2548–2563.
[27] S. Mai, F. Plasser, J. Dorn, M. Fumanal, C. Daniel, L. González, *Coord. Chem. Rev.* **2018**, *361*, 74–97.
[28] P. Kimber, F. Plasser, *Phys. Chem. Chem. Phys.* **2020**, DOI: 10.1039/D0CP00369G.
[29] F. Plasser, *J. Chem. Phys.* **2020**, *152*, 084108.
[30] A. V. Luzanov, O. A. Zhikol, *Int. J. Quantum Chem.* **2010**, *110*, 902–924.
[31] S. Tretiak, S. Mukamel, *Chem. Rev.* **2002**, *102*, 3171–3212.
[32] a) A. Dreuw, M. Head-Gordon, *Chem. Rev.* **2005**, *105*, 4009–4037; b) D. J. Tozer, R. D. Amos, N. C. Handy, B. O. Roos, L. Serrano-Andres, *Mol. Phys.* **1999**, *97*, 859–868; c) D. J. Tozer, *J. Chem. Phys.* **2003**, *119*, 12697–12699.
[33] a) M. E. Casida, D. R. Salahub, *J. Chem. Phys.* **2000**, *113*, 8918–8935; b) A. Dreuw, J. L. Weisman, M. Head-Gordon, *J. Chem. Phys.* **2003**, *119*, 2943–2946; c) A. Vlček, S. Záliš, *Coord. Chem. Rev.* **2007**, *251*, 258–287.
[34] T. Yanai, D. P. Tew, N. C. Handy, *Chem. Phys. Lett.* **2004**, *393*, 51–57.
[35] Y. Tawada, T. Tsuneda, S. Yanagisawa, T. Yanai, K. Hirao, *J. Chem. Phys.* **2004**, *120*, 8425–8433.
[36] a) A. Dreuw, M. Head-Gordon, *J. Am. Chem. Soc.* **2004**, *126*, 4007–4016; b) R. J. Magyar, S. Tretiak, *J. Chem. Theory Comput.* **2007**, *3*, 976–987; c) S. A. Mewes, F. Plasser, A. Dreuw, *J. Chem. Phys.* **2015**, *143*, 171101.
[37] S. A. Mewes, F. Plasser, A. Dreuw, *J. Phys. Chem. Lett.* **2017**, *8*, 1205–1210.
[38] M. Roemelt, M. A. Beckwith, C. Duboc, M.-N. Collomb, F. Neese, S. DeBeer, *Inorg. Chem.* **2012**, *51*, 680–687.
[39] F. Neese, *WIREs Comput. Mol. Sci.* **2012**, *2*, 73–78.
[40] a) J. P. Perdew, *Phys. Rev. B* **1986**, *33*, 8822–8824; b) A. D. Becke, *Phys. Rev. A* **1988**, *38*, 3098–3100; c) F. Neese, G. Olbrich, *Chem. Phys. Lett.* **2002**, *362*, 170–178.
[41] a) D. Andrae, U. Haussermann, M. Dolg, H. Stoll, H. Preuss, *Theor. Chim. Acta* **1990**, *77*, 123–141; b) F. Weigend, R. Ahlrichs, *Phys. Chem. Chem. Phys.* **2005**, *7*, 3297–3305.
[42] F. Weigend, *Phys. Chem. Chem. Phys.* **2006**, *8*, 1057–1065.

[43] a) S. Grimme, S. Ehrlich, L. Goerigk, *J. Comput. Chem.* **2011**, *32*, 1456–1465; b) S. Grimme, R. Huenerbein, S. Ehrlich, *ChemPhysChem* **2011**, *12*, 1258–1261.
[44] S. Hirata, M. Head-Gordon, *Chem. Phys. Lett.* **1999**, *314*, 291–299.
[45] a) A. D. Becke, *J. Chem. Phys.* **1993**, *98*, 5648–5652; b) C. Lee, W. Yang, R. G. Parr, *Phys. Rev. B* **1988**, *37*, 785–789; c) F. Neese, F. Wennmohs, A. Hansen, U. Becker, *Chem. Phys.* **2009**, *356*, 98–109.

Received: December 6, 2019